Thermochimica Acta, 238 (1994) 1–16
Elsevier Science B.V., Amsterdam
SSDI 0040-6031(93)0157-N

Calorimetric analysis of liquid–liquid phase separation

J. Arnauts *, R. De Cooman, P. Vandeweerdt, R. Koningsveld and H. Berghmans

Laboratory for Polymer Research, Catholic University of Leuven, Celestijnenlaan 200F, B-3001 Heverlee (Belgium)

(Received 16 May 1993; accepted 21 October 1993)

Abstract

It is shown that differential scanning calorimetry may be used to determine miscibility gaps in micromolecular as well as in macromolecular systems. The first deviation of the signal from the base line is indicative of the onset of liquid–liquid phase separation and allows determination of the cloud-point curve. The area of the endo- or exothermic signal is related to the heat of demixing and may be analysed to supply information about the enthalpic part of the pair-interaction parameter. The method is tested on the systems water/nicotine and *n*-butanol/poly(methyl methacrylate).

INTRODUCTION

It is usual to treat partial miscibility on the basis of free enthalpy (Gibbs free energy) which, when plotted against concentration for a binary liquid, exhibits a plait under the conditions of pressure and temperature in which the system is stable as a two-phase mixture. A schematical example is shown in the lower part of Fig. 1, a familiar feature in any textbook on physical chemistry. A change in pressure and/or temperature may cause a homogeneous system to split up into two phases. The coexisting-phase concentrations are defined by the double tangent and, bringing them together in a phase diagram, one obtains the equally familiar picture shown in the upper part of Fig. 1.

There are various ways in which the binodal (the envelope of the two-phase region) can be determined experimentally. For instance, working at constant pressure, one might heat a mixture up to a temperature above the miscibility gap, homogenize it, and then gradually cool it until the first cloudiness indicates the onset of phase separation. Alternatively, one might stir a two-phase mixture within the miscibility gap until thermal equilibrium has been reached, after which the phases are allowed to settle

* Corresponding author.

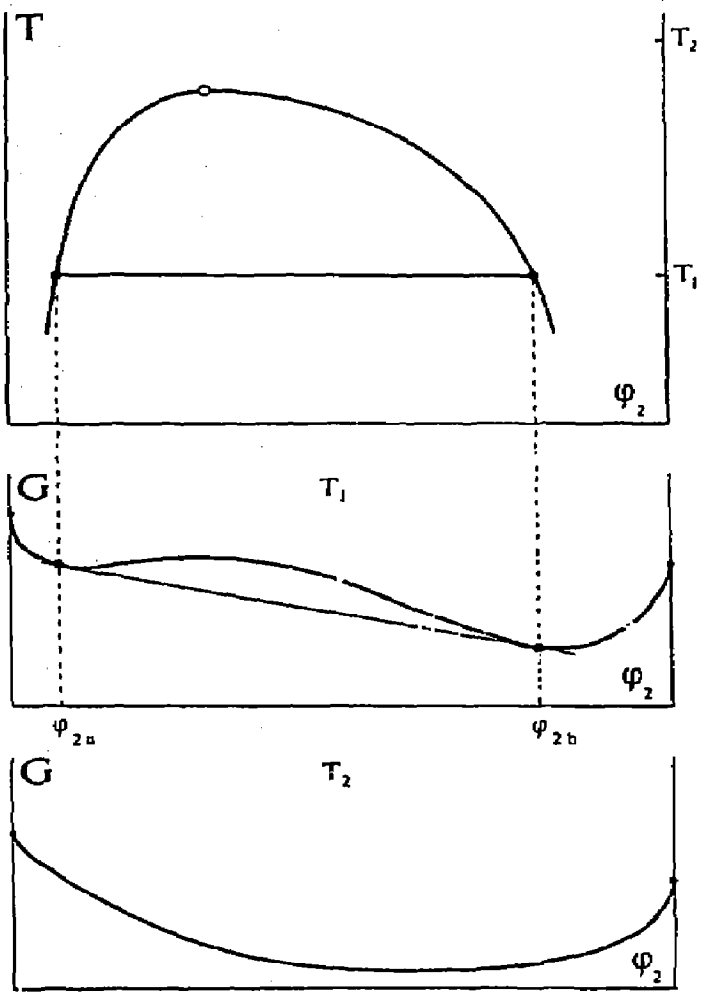

Fig. 1. Upper. Miscibility gap for a binary liquid system: coexisting phases and tie line at T_1, ●—●; critical point, ○.
Middle. Free enthalpy (Gibbs free energy) G plotted against composition φ_2 for T_1, defining equilibrium between phases a and b.
Lower. $G(\varphi_2)$ for a homogeneous liquid mixture, e.g. at T_2 (schematic).

and segregate. Subsequent analysis of the phases then yields the compositions of the two coexisting phases at the temperature involved.

This paper concentrates on another alternative: the use of the enthalpy change that occurs when a binary liquid mixture separates into two liquid phases. The principle is illustrated in Fig. 2. We note that h', the enthalpy of the homogeneous system, is larger than that of the two-phase mixture h'', and, consequently, the enthalpy jump accompanying demixing should be detectable with calorimetric methods. Differential scanning calorimetry (DSC) could therefore provide an alternative method for the determination of miscibility gaps. Once DSC had removed the time-consuming character of earlier calorimetric techniques, it seemed worthwhile to develop further

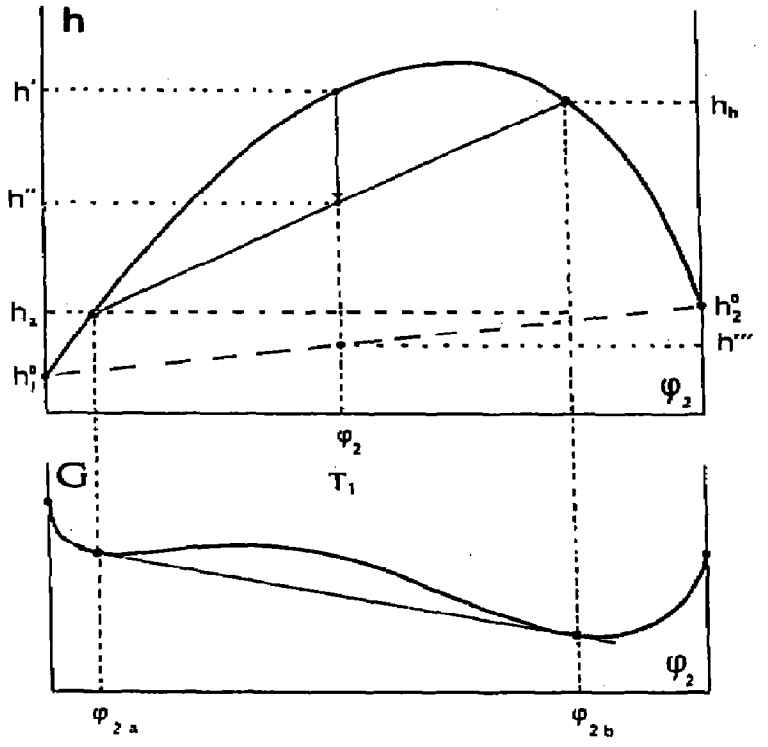

Fig. 2. Upper. Enthalpy h vs. composition φ_2. The enthalpies of pure components 1 and 2 are $h_1^{\ominus}$ and $h_2^{\ominus}$. The enthalpy of mixing Δh (eqn. (7)) equals $h' - h'''$ at φ_2; the enthalpy of demixing is $h' - h''$ for separation of system φ_2 into phases φ_{2a} and φ_{2b}.
Lower. Free enthalpy G vs. φ_2 for the two phase system a/b (schematic).

the principles of the method. Figure 3 clearly demonstrates that the enthalpy jump that takes place during demixing is easily measurable by DSC in micromolecular as well as in macromolecular solutions. The main condition is a sufficiently large enthalpy jump. Moreover, the DSC signal contains additional information and the possibilities of this technique are analysed in this study.

PRINCIPLES OF THE METHOD

In order to check whether the method may be expected to yield significant results, we first put the schematical figures, Figs. 1 and 2, on a more quantitative basis. To this end we introduce an expression for $\Delta G(T, \varphi_2)$ which is a useful tool in the description of miscibility gaps. It is an extension of the rigid-lattice expression developed independently by Staverman and Van Santen [1, 2], Huggins [3, 4] and Flory [5]. For a binary system, this expression ΔG for the free enthalpy of mixing of n_1 and n_2 moles of components 1 and 2 reads

$$\Delta G/(NRT) = (\varphi_1/m_1) \ln \varphi_1 + (\varphi_2/m_2) \ln \varphi_2 + g\varphi_1\varphi_2 \qquad (1)$$

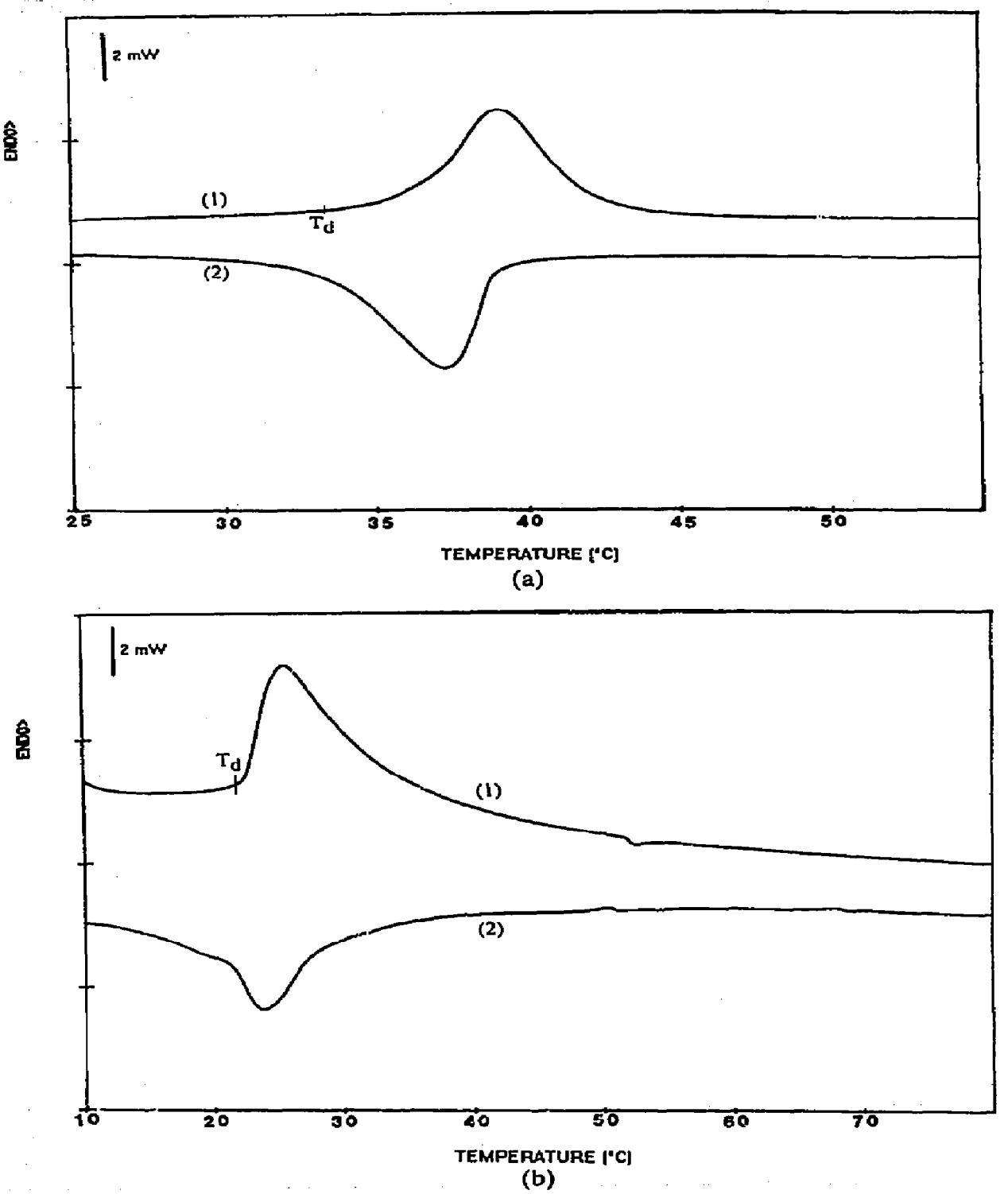

Fig. 3. DSC scans of (a) water/poly(vinylmethylether) (mass fraction $w_2 = 0.07$) and (b) water/triethylamine ($w_2 = 0.35$) both performed at 5°C min^{-1}. (1) Heating experiment; (2) cooling experiment.

This equation will be referred to in this paper as the FHS equation. The total number of lattice sites is $N = n_1 m_1 + n_2 m_2$, and RT has the usual meaning. Each molecule occupies m_i sites and φ_i represents the volume fraction of component i. The volume fraction is defined by $\varphi_i = n_i m_i / N$.

In the extended FHS version, the pair-interaction parameter g is given by [6–8]

$$g = g_s + (g_{s1} + g_h/T)/(1 - c\varphi_2) \tag{2}$$

were g_s and g_{s1} are parameters, g_h is proportional to z_2, the average number of nearest neighbours of a molecule or repeating unit in component 2, and c is defined as

$$c = 1 - z_2/z_1 \tag{3}$$

In this study we do not further specify the coordination numbers z_1 and z_2, and also treat c as a parameter. Setting $c = 0$, we recover the original FHS equation, and the interaction function now reads

$$g = g_s + g_h/T \tag{2a}$$

in which we have dropped the superfluous g_{s1}. Setting, in addition, both m_1 and m_2 equal to unity, we reduce eqn. (1) to the Van Laar/Bragg–Williams expression. The variables φ_i are then identical to mole fractions. A polymer solution is characterized by $m_1 = 1$ and $m_2 \gg 1$. It can be demonstrated that the volume fraction may often be replaced by the mass fraction, and m_2 be set equal to the ratio of polymer and solvent molar mass [9].

Using standard procedures, we can calculate phase diagrams for micromolecular systems ($m_1 = 1$, $m_2 = 1$) such as those shown in Fig. 4 for various sets of (g_s, g_h) values. Note that the miscibility gaps calculated in this way are symmetrical about the critical concentration, $\varphi_{2c} = 1/2$, and that the curvature at the extremum depends on the choice of g_s and g_h. Very small curvatures are often observed and would call for unrealistic values of g_h, the latter quantity being defined within the model to be of the order of a Van der Waals energy. Neglecting non-classical critical behaviour, we may rely on the fact that the pair-interaction parameter is often found to depend on concentration, which supplies an alternative and, for the present purposes, sufficient way of dealing with flat-topped miscibility gaps. It has been shown that multiple critical behaviour of the system may then play a role, and can be adequately dealt with, writing [10]

$$g = g_s + g_h/T + g_1\varphi_2 + g_2\varphi_2^2 \tag{4}$$

It is seen in Fig. 4 that introduction of the values $g_1 = -4/3$ and $g_2 = +4/3$ produces the desired effect of 'flatness'.

The enthalpy of mixing Δh can be derived from eqns. (1) and (2) with the Gibbs–Helmholtz expression which yields

$$\Delta h/(NR) = g_h\varphi_1\varphi_2/(1 - c\varphi_2) \tag{5}$$

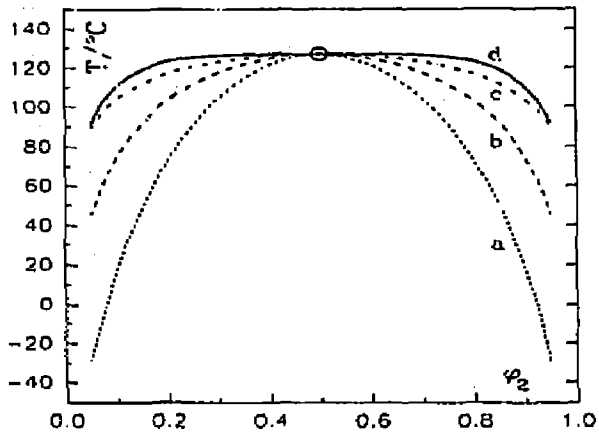

Fig. 4. Miscibility gaps in a symmetrical system ($m_1 = 1$, $m_2 = 1$) calculated with eqns. (1) and (2); critical point, O

	g_s	g_h/K	g_1	g_2
Curve a	0	800		
Curve b	−3	2000		
Curve c	−10.5	5000		
Curve d	−5	3067	−4/3	4/3

Figure 5 shows $\Delta h(\varphi 2)$ curves calculated with eqn. (5) for the four cases in Fig. 4.

On inspection of Fig. 2, it can easily be derived that q_d, the heat of demixing accompanying a separation of system φ_2 into two phases with compositions φ_{2a} and φ_{2b}, is related to the corresponding enthalpy difference, $h' - h''$ by [11]

$$q_d = -(\Delta h' - \Phi_a \Delta h_a - \Phi_b \Delta h_b) \tag{6}$$

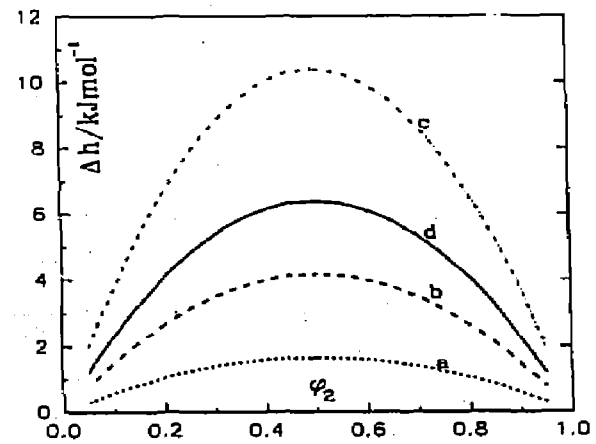

Fig. 5. Enthalpy of mixing calculated using eqns. (5) ($c = 0$) for the four systems of Fig. 4.

where each of the quantities Δh is defined by

$$\Delta h = h - \sum \varphi_i h_i^{\ominus} \tag{7}$$

and where

$$\Phi_a = (\varphi_{2b} - \varphi_2)/(\varphi_{2b} - \varphi_{2a})$$

$$\Phi_b = (\varphi_2 - \varphi_{2a})/(\varphi_{2b} + \varphi_{2a})$$

Introducing eqn. (5) we arrive at

$$q_d/(NR) = g_h(\varphi_{1a}\varphi_{2a}\Phi_b/C_a + \varphi_{1b}\varphi_{2b}\Phi_a/C_b - \varphi_1\varphi_2/C_1) \tag{8}$$

with

$$C_k = 1 - c\varphi_{2k}$$

the index k indicating a, b or the initial one-phase system with volume fraction φ_2 ($\varphi_1 = 1 - \varphi_2$).

It should be mentioned here that eqn. (5) represents $\Delta h(\varphi_2)$ curves that do not exhibit a point of inflexion, i.e. the behaviour represented by Figs. 2 and 5. The sign of g_h determines whether Δh is positive or negative and the curves show either positive or negative curvature over the full concentration range. The majority of reported data displays this behaviour, but exceptions are known [12, 13]. For example, both positive and negative values of Δh have been reported for the water/acetone system, depending on the c... position of the mixture [14]. We may mention, in passing, that this phenomenon can be simulated with eqn. (4), provided the coefficients g_1 and/or g_2 are made temperature dependent [15, 16]. However, as far as the determination of cloud points is concerned, the shape of $\Delta h(\varphi_2)$ hardly matters and it is in the interpretation of the complete DSC signal that caution is needed in this respect.

Figure 6 shows q_d plotted against T at $\varphi_2 = 0.5$ for the four simulated

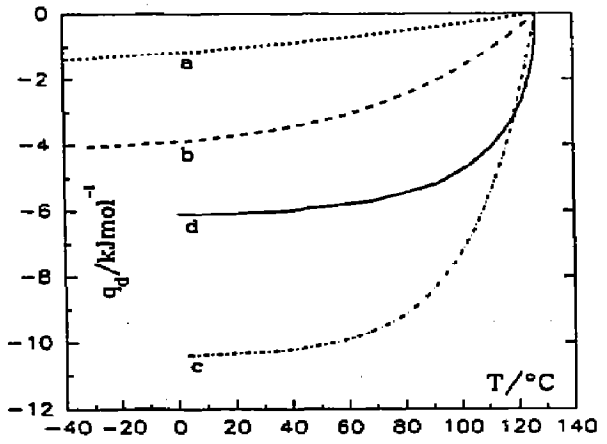

Fig. 6. Heat of demixing q_d vs. temperature for systems a–d in Fig. 4 at the critical fraction, $\varphi_{2c} = 0.5$.

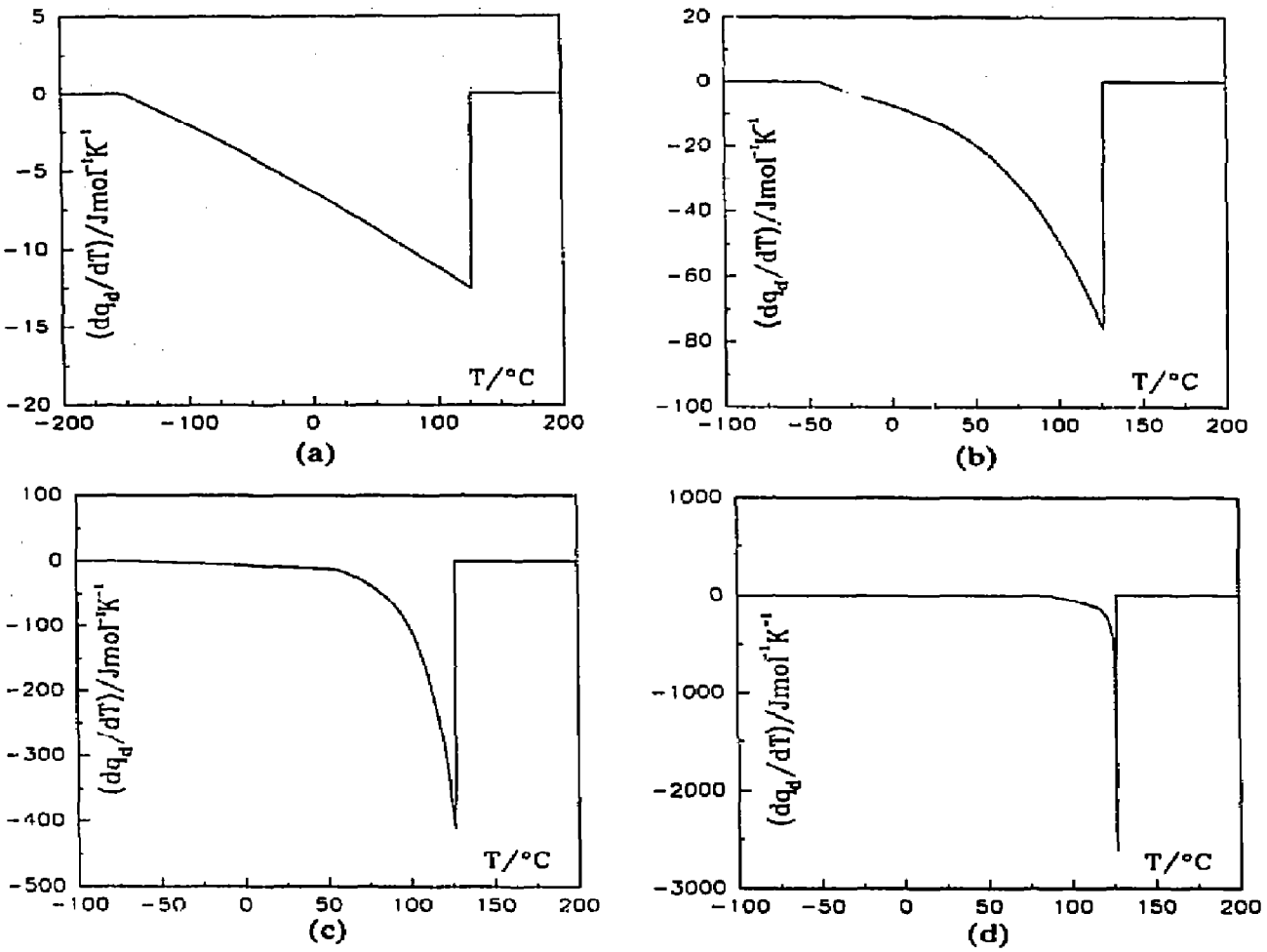

Fig. 7. Simulations of DSC scans for the systems (a)–(d) in Fig. 4.

binodals in Fig. 4. It is obtained [11, 17] by calculation of the coexisting-phase compositions φ_{2a} and φ_{2b} for a given temperature and introduction of these values in eqn. (8). A DSC scan corresponds to the derivative of q_d with respect to temperature which we can derive from the curves in Fig. 6. Figure 7a–d shows simulations obtained by graphical differentiation of the q_d curves in Fig. 6. It is seen that these curves narrow markedly with a decrease in the curvature of the binodal at its extreme. The peak height increases when the binodal becomes flatter (Fig. 7a–c) which reflects the increasing value of g_{1i} that we had to introduce in order to flatten the binodal. If the binodal is very flat (Fig. 4, curve d), most of the heat of demixing is set free at temperatures close to that of the maximum of the binodal. We note the same pattern in comparing Fig. 7a–c, and may conclude that the shape of a DSC scan may be expected to supply useful information about the pair-interaction parameter. The discontinuity at the end of the signal in Fig. 7a,b is due to the calculation procedure in which it

is difficult to judge the phase-separation temperature down to which the calculation should be continued.

APPLICATION TO ACTUAL SYSTEMS

In the application of model expressions like the FHS equation, it is invariably found that thermodynamic properties of actual mixtures cannot be described adequately with such a simple model. One factor is the difference in molecular size and shape between the constituents which, being related to a disparity in coordination number, leads to a concentration dependence of the pair interaction parameter as expressed by eqn. (2). Moreover, it can be shown that the parameter g_s is also affected by differences in the number of nearest neighbours and should be expected to depend on concentration [8, 18]. We summarize this feature

$$g = g_s + g_{s\varphi}\varphi_2 + (g_{s1} + g_h/T)/(1 - c\varphi_2) \quad (9)$$

and use $g_{s\varphi}$ as an adaptable parameter. There are other reasons for the concentration dependence of g, namely disparity in free volume, or specific interactions. Being interested here in general principles, we will restrict further discussion to systems in which eqns. (2) and (9) have been found to lead to acceptable descriptions of the cloud-point curve and, hence, we must assume that eqns. (5) and (8) will also be adequate.

The water/nicotine system

The water/nicotine system has long been known to exhibit a closed miscibility gap [19]. Figure 8 shows data taken by DSC which compare favourably with the literature values [20]. The single DSC point at the top overshoots, probably because of kinetic problems resulting from the rate of diffusion of heat into the sample and the rate of remixing. Figure 9 displays a DSC scan obtained on heating. The two endothermic signals correspond to the demixing when the closed two-phase domain is entered and the remixing when passing through the upper part of this domain, respectively. The endothermic character of both transitions illustrates the difference in sign of the heat of mixing of nicotine and water. Within the concentration range of the demixing domain, mixing is exothermic at low temperature and becomes endothermic at higher temperature.

The concentration variable appearing in eqns (1)–(9) is the volume fraction, an inconvenient quantity in practical applications. It has been shown that the volume fraction may, without loss of significance, be replaced by the mass fraction [9]. The relative chain lengths m_1 and m_2 may then be calculated with $m_i = M_i/M_1$, where M_i and M_1 are the molar masses of the constituents i and 1 respectively.

The critical point is located at a nicotine mass fraction $w_2 = 0.322$ which points to molecular asymmetry in the system ($m_2 > m_1$) [5, 21]. Indeed, the

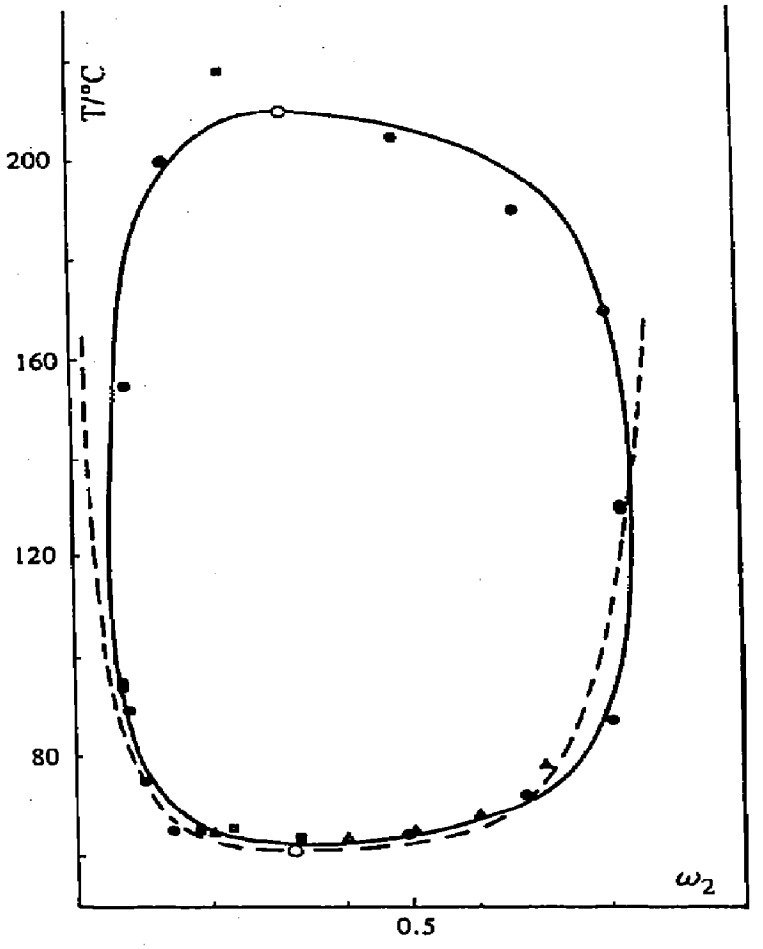

Fig. 8. Miscibility gap in the system water/nicotine: ●, data by Hudson [19]; ○, critical point; ■, DSC [20]; ▲, optical observation [20]. The curves represent simulations with eqns. (1) and (9); parameter values: $m_1 = 1$, $m_2 = 9$

	c	g_h/K	$10^4 \times g_s$/K	g_s	$g_{s\varphi}$	g_{s1}
Solid line	0.5	−1258.2	−7.7698	−0.12397	−0.42364	7.5623
Broken line	0.2291	−277.0	0	−6.653	−1.6511	0

FHS model places the critical concentration at $w_{2c} = 0.25$. This result is obtained by assigning the values 1 and 9 to m_1 and m_2, respectively. Because we are working on the basis of the mass fraction, the ratio m_2/m_1 may be set equal to the ratio of the molar masses of nicotine and water. Obviously, further corrections are needed in order to let calculated and measured critical concentrations coincide; for this, eqn. (9) can be used. However, it must be realized that eqn. (9) requires Δh to be independent of T and is, therefore, incapable of covering the complete binodal. Nevertheless, simulation of the lower part of the binodal is possible, as is seen in Fig.

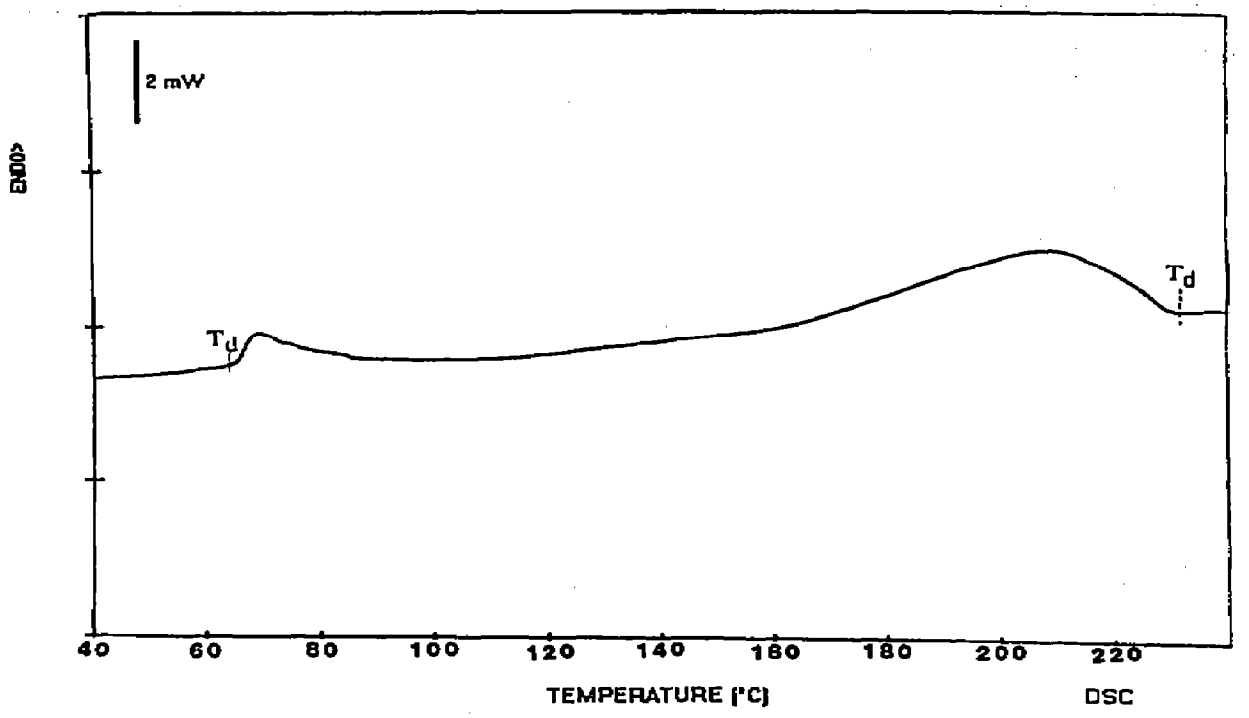

Fig. 9. DSC scan of water/nicotine ($w_2 = 0.33$) performed at 10°C min^{-1} (heating experiment).

8. Following the procedure explained in the preceeding section, we calculate q_d (Fig. 10) and find that the latter curve agrees only qualitatively with the relevant part of the DSC scan. In accordance with the flat lower part of the binodal, we find that most of the heat of demixing is released

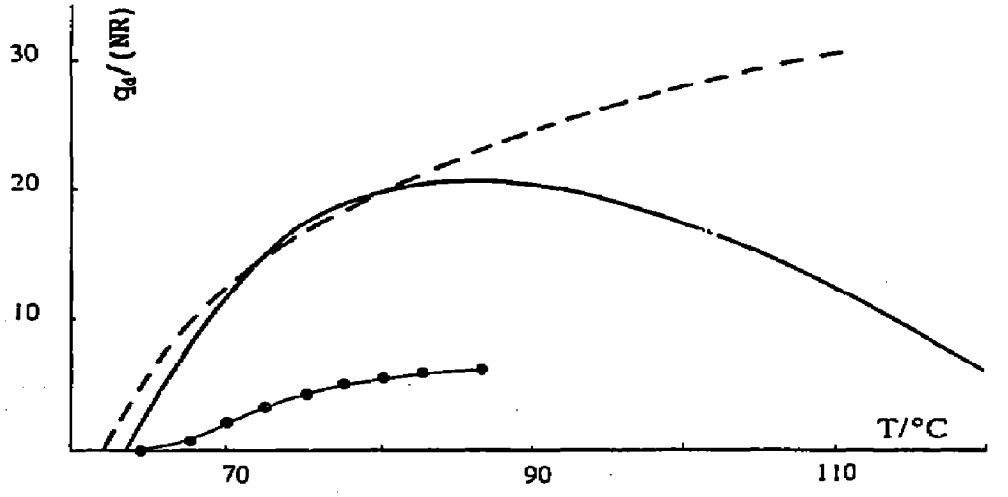

Fig. 10. Heat of demixing calculated with eqn. (8) in connection with eqn. (9) (broken curve) and eqn. (10) (curve) (details in caption of Fig. 8). Integrated DSC scans: ●—●—●.

just above the demixing temperature. Yet, the measured and calculated q_d curves differ significantly, the calculated $q_d(T)$ effect being about four times larger than the values from the DSC scan. Various reasons may be advanced to explain the deviations. First, the model used in the description may be inadequate. However, the lower part of the miscibility gap is quite well covered by the (broken) curve and it seems more likely that the discrepancy derives from characteristics of the experimental technique. For instance, the dynamic characteristics of the DSC measurements and the kinetics of the demixing process will yield two endothermic signals extending over a wider temperature range than will result from measurements under thermal equilibrium. This will flatten these signals, making an accurate quantitative integration difficult.

Coming back to the model used, it is clear that the inadequate temperature dependency of g cannot be held responsible for the deviations, as is demonstrated by the curve drawn in Fig. 8, which leads to the corresponding curve in Fig. 10. There we see that the first part of the calculated q_d is not much affected if an improved $g(T)$ function is used. The simplest conceivable improvement consists of a term which is linear in temperature [15]

$$g = g_s + g_{s\varphi}\varphi_2 + (g_{sl} + g_h/T + g_x T)/(1 - c\varphi_2) \qquad (10)$$

where g_x is a parameter.

The drawn curve in Fig. 8 demonstrates the viability of the manoeuvre. Yet, it is seen in Fig. 10 that the first part of the $q_d(T)$ curve is hardly affected. The improvement resides in the description of the top part of the binodal and the discrepancy remains in the temperature range of the DSC scan. The remarks made above about the deviation between the measured and the calculated q_d curves are further illustrated in Fig. 11 which shows

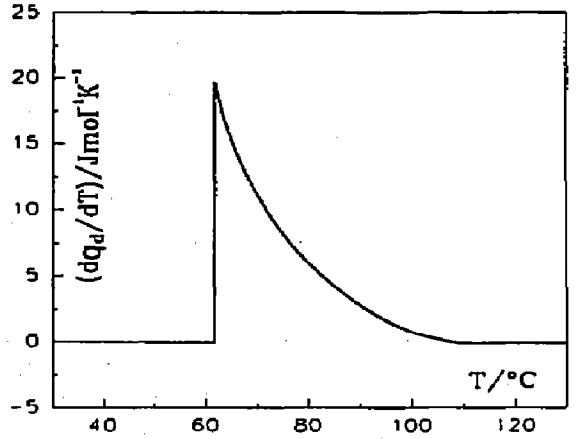

Fig. 11. Simulation of the DSC scans of Fig. 9 by the differentiation of the $q_d(T)$ curve of Fig. 10.

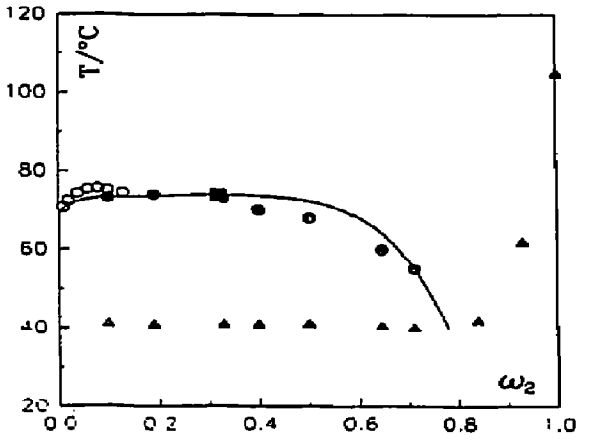

Fig. 12. Miscibility gap in the system *n*-butanol/PMMA: ●, DSC, ○, optical observation. The curve represents a simulation with eqns. (1) and (2). Parameter values: $g_{1h} = 144.3$ K; $c = 0.58$; $g_s = 0.232$; $g_{s1} = 0.233$. Characteristics of the polymer: $M_w = 88$ kg mol^{-1}; $M_w/M_n = 1.05$; $M_z/M_w = 1.04$. ■, Calculated critical point; ▲, concentration dependence of T_g (DSC).

the calculated DSC scan derived from Fig. 10. The heat flow is greatest at the beginning of the demixing process and cannot be followed in the present DSC setup (see Fig. 9).

The n-*butanol/poly(methyl methacrylate) system*

The miscibility gap measured by DSC for solutions of a sample of poly(methyl methacrylate) (PMMA) in *n*-butanol is shown in Fig. 12 [11]. At low polymer concentration, the DSC signal is too small to be useful for a significant determination. We established the cloud points in that region by cooling homogeneous solutions and observing the onset of the phase separation or the first cloudiness. The two sets of data connect quite reasonably, in view of the different methods used.

The curve in Fig. 12 was calculated with eqn. (2) using a procedure developed earlier for so-called quasi-binary solutions [9, 22, 23]. This was necessary because the polymer sample, although having a narrow molar mass distribution, still cannot be treated as a single component. In this case, it was not necessary to resort to expressions more involved than eqn. (2). We note that the flat top of the cloud-point curve is well described and, hence, may expect the DSC signal to point to a release of most of the heat of demixing right under the cloud point. As far as the calculation goes, this feature is well confirmed by the $q_d(T)$ curve and the simulated DSC signal for a mass fraction $w_2 = 0.3$ displayed in Figs. 13 and 14, obtained by application of the procedures described above.

The experimental DSC scans are shown in Fig. 15. They are more complex than those of the micromolecular mixtures illustrated in Figs. 3

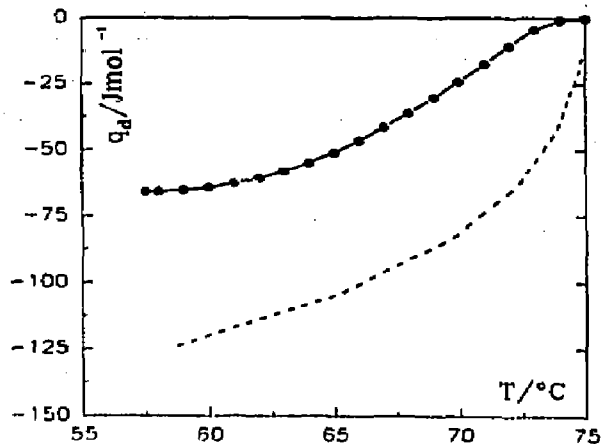

Fig. 13. Heat of demixing calculated with eqn. (8) and eqns. (1) and (2); ●—●—●, integrated DSC scans for $w_2 = 0.3$.

and 9 because the glass transition of the polymer interferes with the miscibility gap [24–26].

Although the experimental heat of demixing occurs over a larger temperature range than is predicted by the model, it is still true that most of it is set free immediately below the cloud point. The difference between the measured and calculated DSC scans may partly be due to the dynamic character of the DSC measurements, which may be expected to show up more markedly in the polymer system than in the micromolecular mixture discussed above. However, the marked flatness of the cloud-point curve may be the main reason why the disparity between the calculated and the experimental q_d curves is now smaller than in the water/nicotine system (a factor of 2 versus 4). Clarification of this can be obtained by repeating the measurements at a significantly smaller degree of heating. Some

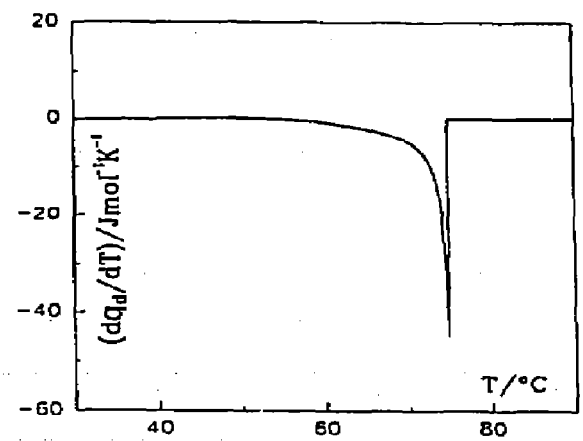

Fig. 14. Simulation of the DSC scan of Fig. 15 by differentiation of the $q_d(T)$ curve in Fig. 13.

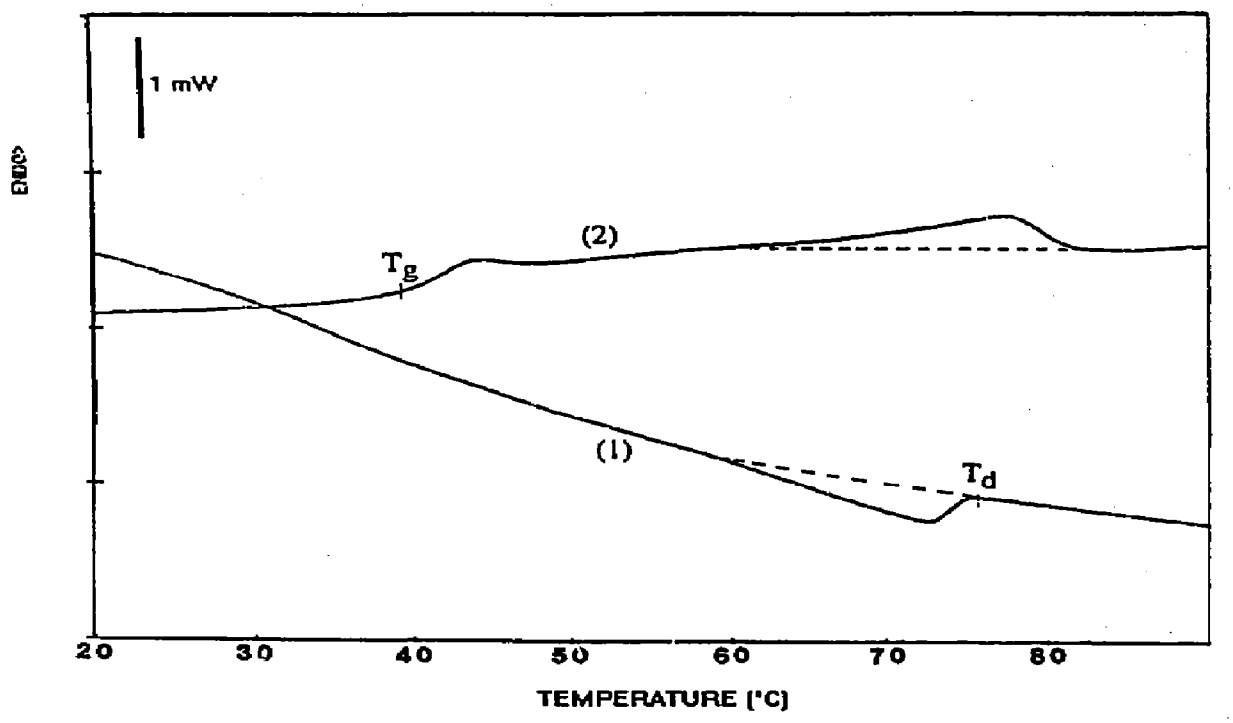

Fig. 15. DSC scans of *n*-butanol/PMMA ($w_2 = 0.33$) performed at 5°C min^{-1} [26]: (1) cooling experiment; (2) heating experiment.

preliminary measurements with a Setaram calorimeter indicate that this might indeed be the explanation.

ALTERNATIVE EVALUATION OF THE DSC SCAN

The analysis presented so far consists of an after-the-fact comparison of the measured and predicted DSC scans, the prediction resting on knowledge of the cloud-point curve and of the parameters in the ΔG equation. It would, however, be interesting to investigate whether the DSC signal itself contains enough information to allow conclusion about the pair-interaction function. This includes integration of the DSC scan, and fitting of the resulting $q_d(\varphi_2)$ curve to sets of (c, g_h) values (see eqn. (8)). This procedure requires some care with respect to normalization, because the integrated DSC scan is in J g^{-1}, whereas the model has q_d in J mol^{-1} [11].

For the water/nicotine system, the best agreement between the calculated relationship and the experimental data is found with $h = -100$ K and $c = -2.5$, values that are different from those that had to be introduced in the simulation of the demixing curve (Fig. 8). This deviation between the two sets of parameters may find its origin in the difference between the calculated and measured q_d values (Fig. 10). Treatment of the DSC signal

in this fashion obviously cannot lead to unambiguous values for the interaction parameters. However, it is clear that a concentration independence of g can be ruled out and, in this sense, the analysis is useful.

ACKNOWLEDGEMENTS

The authors are indebted to the IWONL for a fellowship to R.D.C. and P.V. and to the National Fund for Scientific Research for a fellowship to J.A. Financial support by the National Fund for Scientific Research and the Ministry of Scientific Programmation through the IUAP-16 is gratefully acknowledged.

REFERENCES

1 A.J. Staverman and J.H. Van Santen, Recl. Trav. Chim. Pays-Bas, 60 (1941) 76.
2 A.J. Staverman, Recl. Trav. Chim. Pays-Bas, 60 (1941) 640.
3 M.L. Huggins, J. Chem. Phys., 9 (1941) 440.
4 M.L. Huggins, Ann. N.Y. Acad. Sci., 43 (1942) 1.
5 P.J. Flory, J. Chem. Phys., 9 (1941) 660; 10 (1942) 51.
6 A.J. Staverman, Recl. Trav. Chim. Pays-Bas, 56 (1937) 885.
7 A.J. Staverman, Ph.D. Thesis, University of Leiden, 1938.
8 R. Koningsveld, L.A. Kleintjens and A.M. Leblans-Vinck, J. Phys. Chem., 91 (1987) 6423.
9 R. Koningsveld and A.J. Staverman, J. Polym. Sci., Part A2, 6 (1968) 305, 325, 349.
10 K. Solc, L.A. Kleintjens and R. Koningsveld, Macromolecules, 17 (1984) 573.
11 P. Vandeweerdt, Ph. D. Thesis, Structure Formation in Solutions of Atactic Poly(methyl methacrylate), Ph.D. Thesis, University of Leuven, 1993.
12 J.J. Christensen, R.W. Hanks and R.M. Izatt, Handbook of Heats of Mixing, Wiley, New York, 1982.
13 J.J. Christensen, R.W. Hanks and R.M. Izatt, Handbook of Heats of Mixing, Supplementary Volume, Wiley, New York, 1988.
14 H.T. French, J. Chem. Thermodyn., 21 (1989) 801.
15 K. Solc and R. Koningsveld, J. Phys. Chem., 96 (1992) 4056.
16 S. Vanhee, R. Koningsveld, H. Berghmans and K. Solc, J. Polym. Sci., Polym. Phys. Ed., submitted for publication.
17 J. Arnauts, Thermal Transitions and Gelation of Solutions of Atactic Polystyrene, Ph.D. Thesis, University of Leuven, 1989.
18 A.J. Staverman, in L.A. Kleintjens and P.J. Lemstra (Eds), University of Integration of Fundamental Polymer Science and Technology, Vol. I, Elsevier, London, 1986, p. 19.
19 C.S. Hudson, Z. Phys. Chem., 47 (1904) 113.
20 R. De Cooman, Study of Liquid–Liquid Demixing in Binary Systems, Ph.D. Thesis, University of Leuven, in preparation.
21 J.D. Van Der Waals and Ph. Kohnstamm, Lehrbuch der Thermodynamik, Vol. II, Barth, Leipzig, 1912.
22 R. Koningsveld, Chem. Zvesti, 26 (1972) 263.
23 R. Koningsveld and K. Solc, Collect. Czech. Chem. Commun., in press.
24 J. Arnauts and H. Berghmans, Polym. Commun., 28 (1987) 66.
25 J. Arnauts and H. Berghmans, in W. Burchard and S.B. Ross-Murphy (Eds.), Polymer Networks, Elsevier Applied Science, London, 1990, Chapter 3, p. 35.
26 P. Vandeweerdt, H. Berghmans and Y. Tervoort, Macromolecules, 24 (1991) 3547.